Secondary proximity effect in a side-coupled double quantum dot structure

Jia-Ning Wang,[1,2] Yong-Chen Xiong ,[1,2,*] Wang-Huai Zhou,[1,2] Tan Peng ,[1,2,3] and Ziyu Wang[3,†]

[1]*Shiyan Key Laboratory of Quantum Information and Precision Optics, and School of Mathematics, Physics and Optoelectronic Engineering, Hubei University of Automotive Technology, Shiyan 442002, People's Republic of China*

[2]*Hubei Key Laboratory of Energy Storage and Power Battery, and Collaborative Innovation Center for Optoelectronic Technology, Hubei University of Automotive Technology, Shiyan 442002, People's Republic of China*

[3]*The Institute of Technological Sciences, Wuhan University, Wuhan 430072, People's Republic of China*

(Received 23 October 2023; revised 17 January 2024; accepted 14 February 2024; published 27 February 2024)

Semiconductor quantum dots in close proximity to superconductors may provoke localized bound states within the superconducting energy gap known as the Yu-Shiba-Rusinov state, which is a promising candidate for constructing Majorana zero modes and topological qubits. Side-coupled double quantum dot systems are ideal platforms revealing the secondary proximity effect. Numerical renormalization group calculations show that if the central quantum dot can be treated as a noninteracting resonant level, it acts as a superconducting medium due to the ordinary proximity effect. The bound state in the side dot behaves as the case of a single impurity connected to two superconducting leads. The side dot undergoes a quantum phase transition between a spin-singlet state and a doublet state as the Coulomb repulsion, the interdot coupling strength, or the energy level sweeps. Phase diagrams indicate that the phase boundaries could be well illustrated by $\Delta \approx cT_{K2}$ in all cases, where Δ is the superconducting gap, T_{K2} is the side Kondo temperature and c is of the order 1.0. These findings offer valuable insights into the secondary proximity effect, which is a promising approach for realizing superconducting couplings between quantum dots and reducing the random-disorder potential via quantum interferences.

DOI: 10.1103/PhysRevB.109.064518

I. INTRODUCTION

When a semiconductor quantum dot (QD) is attached by a superconductor electrode, interactions between magnetic moments in the QD and Cooper pairs in the lead [1,2] may result in quasiparticle excitations and low-energy bound states inside the superconducting gap, and the so-called Yu-Shiba-Rusinov (YSR) bound state, or simply Shiba state, could be found in the local density of states of the QD [3–5]. Recently, this field has attracted significant attention since it provides many opportunities for systematic investigations of Majorana zero modes (MZMs) within which fault-tolerant quantum computation could be implemented [6–11]. Furthermore, such hybrid superconductor-semiconductor systems offer unique access to design and construct superconducting quantum devices, such as topological qubits [12,13], effective topological superconductor [14–18], thermoelectric engine [19], thermal quantum interference proximity transistor [20], spin-orbit-coupling semiconductor nanowires [6,21–25], superconducting-topological insulator hybrids [26–28], superconducting two-dimensional (2D) devices [29–31], and so on.

Basically, the YSR state is induced by the proximity effect [32], where, if a superconducting material is put into contact with a nonsuperconducting one, the electron pairing correlations can propagate into the nonsuperconducting part, inducing superconductinglike properties near the interface [33]. Previous works mainly concentrated on the direct proximity effect occurring on those architectures which are connected firsthand to the superconducting material [34–48]. However, it would be quite interesting if one nano-object (subsystem I) is separated by a nonsuperconducting object (subsystem II) from the superconducting part. Little is known about the physical picture of the related secondary proximity effect, viz., YSR state on subsystem I. Expectantly, such a secondary proximity effect may show great importance in realizing superconducting couplings between QDs [49], which can be used to implement the Bell inequality test [50,51] and has potential applications in quantum cryptography [52] and quantum teleportation [53]. Furthermore, such a tripartite structure is expected to reduce the problem of random-disorder potential in the process of implementing MZMs via quantum interferences [49,54–57].

II. MODEL AND METHOD

In this work, we consider a side-coupled double quantum dot (SCDQD) device connected to two superconducting leads (see Fig. 1), which is the simplest model that may present the secondary proximity effect. In this system, the central QD (QD1) is sandwiched between the superconducting source (S) and drain (D) electrodes, while the side QD (QD2) only connects directly to QD1 through interdot hopping t. The related second quantized Hamiltonian is given as

*xiongyc_lx@huat.edu.cn

†zywang@whu.edu.cn

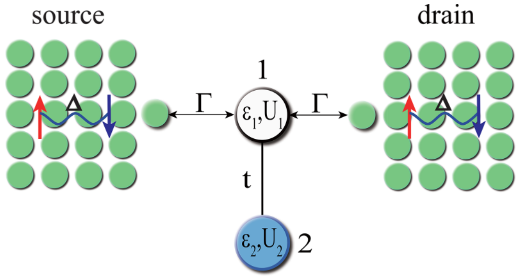

FIG. 1. Schematic illustration of the SCDQD structure connected to the superconducting electrodes. QD1 is the central QD, while QD2 is the side QD. ε_i and U_i are the energy levels and the on-site Coulomb repulsion of the ith QD, respectively. Γ is the hybridization strength between QD1 and the superconducting electrodes. t is the interdot hopping integral.

$\mathcal{H} = \sum_{\nu=S,D} H_\nu + H_{\rm dots} + H_{\rm hyb}$. Here, H_ν illustrates the superconducting electrodes: $H_\nu = \sum_{k\sigma} \varepsilon_{\nu k\sigma} c^\dagger_{\nu k\sigma} c_{\nu k\sigma} - \Delta \sum_k (c^\dagger_{k\uparrow} c^\dagger_{-k\downarrow} + {\rm H.c.})$, where $\varepsilon_{\nu k\sigma}$ is the energy level with respect to the Fermi level, $c^\dagger_{\nu k\sigma}(c_{\nu k\sigma})$ is the creation (annihilation) operator for electrons with wave vector k, spin σ ($=\uparrow$ or $\downarrow$), and Δ is the isotropic superconducting gap parameter. H_{dots} is for electrons on the SCDQD,

$$H_{\rm dots} = \sum_{i\sigma} \varepsilon_i d^\dagger_{i\sigma} d_{i\sigma} + \sum_{i\sigma} U_i n_{i\uparrow} n_{i\downarrow} - t \sum_\sigma (d^\dagger_{1\sigma} d_{2\sigma} + d_{1\sigma} d^\dagger_{2\sigma}), \quad (1)$$

where ε_i and U_i are the single-electron energy and the on-site Coulomb repulsion on the ith ($i = 1, 2$) dot, respectively. $d^\dagger_{i\sigma}$ ($d_{i\sigma}$) creates (annihilates) a local electron on dot i. $n_{i\sigma} = d^\dagger_{i\sigma} d_{i\sigma}$ is the spin $-\sigma$ number operator and t is the interdot hopping integral. Finally, H_{hyb} describes the coupling between QD1 and the superconducting electrodes: $H_{\rm hyb} = \tau \sum_{\nu k\sigma} (c^\dagger_{\nu k\sigma} d_{1\sigma} + {\rm H.c.})$. Here, τ is the tunneling strength, which is assumed to be k and σ independent, and is symmetric with respect to the S and D electrodes.

We use the Wilson's numerical renormalization group (NRG) method [58–61] to solve the model Hamiltonian $\mathcal{H}$. The NRG method is an unbiased nonperturbative method that works perfectly at both zero and finite temperatures, and is a quantitatively reliable technique making a close connection between theoretical and experimental studies [62,63]. In our NRG calculations, we assume the density of states of a wide flat conduction band $\rho_0 = 1/(2\mathbb{D})$, where $\mathbb{D}$ is the half bandwidth. The hybridization function between QD1 and the electrodes could be written as $\Gamma = \pi\rho_0\tau^2$. We take the logarithmic discretization parameter of the leads to be $\Lambda = 3$, and keep nearly 3000 low-lying states within each iteration step. At temperature T, the local density of states (LDOS) of each QD can be defined as

$$A_i(\omega, T) = -\frac{1}{\pi} {\rm Im} G_i(\omega + i\delta). \quad (2)$$

Here, $G_i(\omega + i\delta) = \langle\langle d_{i\sigma}; d^\dagger_{i\sigma}\rangle\rangle_{\omega+i\delta}$ is the Green's function. In the following, we abbreviate $A_i(\omega, T)$ at zero temperature as $A_i(\omega)$.

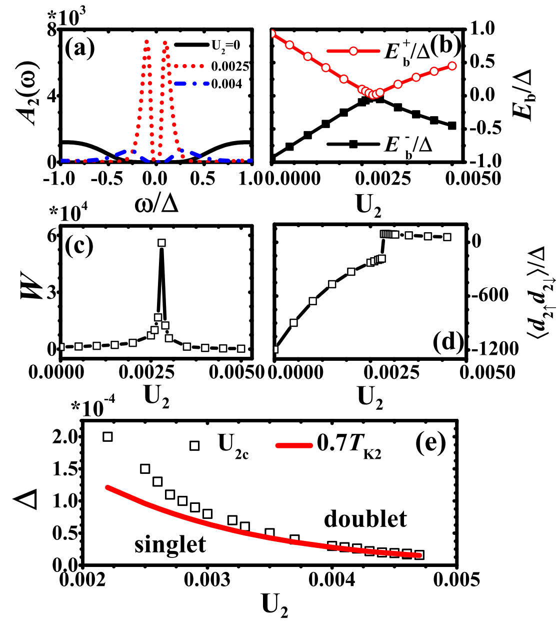

FIG. 2. (a) The LDOS of electrons in QD2 at nearly zero temperature $A_2(\omega)$ in the gap region $[-\Delta, \Delta]$ for various U_2. (b) The energies $E_b^\pm$ and (c) weights W of YSR peaks as functions of U_2. $E_b^\pm$ are scaled by Δ. (d) The expectation value of superconducting order in QD2 $\langle d_{2\uparrow} d_{2\downarrow}\rangle/\Delta$. (e) Phase diagram of the singlet and doublet states as a function of U_2 and Δ. The empty square describes the critical points U_{2c} for fixed Δ. The red line indicates the fitting function given by Eq. (5). The other parameters are given by $U_1 = 0$, $t = 0.002$, $\Gamma = 0.01$, $\Delta = 0.0001$, and $\varepsilon_i = -U_i/2$.

III. RESULTS AND DISCUSSIONS

In Fig. 2(a), we show the LDOS of QD2 $A_2(\omega)$ in the gap regime $[-\Delta, \Delta]$ for fixed $U_1 = 0, t = 0.002, \Delta = 0.0001$ and various U_2. Here, we have chosen $\mathbb{D}$ as the energy unit. For $U_i = 0$, there exists an obvious gap in $A_1(\omega)$, with its edges located at $\pm\Delta$. Meanwhile, a pair of symmetric YSR peaks could be found in $A_2(\omega)$ for different U_2. As U_2 increases, the YSR peaks, viz., the energies of the YSR bound state E_b^+ and E_b^-, move closer to the Fermi surface first if $U_2 < U_{2c}$, then toward the gap edge when $U_2 > U_{2c}$. Correspondingly, the weights of the YSR peaks W increase until U_{2c}, and then they decrease gradually. The whole pictures of $E_b^\pm$ and W varying with U_2 are plotted in Figs. 2(b) and 2(c), respectively.

The above phenomenon indicates a quantum phase transition (QPT) at the critical point $U_{2c} \approx 0.0028$, which finds its counterpart in the expectation value of superconducting order of QD2 $\langle d_{2\uparrow} d_{2\downarrow}\rangle$ shown in Fig. 2(d). It is seen that $|\langle d_{2\uparrow} d_{2\downarrow}\rangle|$ is large for $U_2 < U_{2c}$, since the YSR state can be considered as a linear combination of the empty and doubly occupied states [64]. When U_2 exceeds U_{2c}, $|\langle d_{2\uparrow} d_{2\downarrow}\rangle|$ drops to a smaller value, for U_2 favors the singly occupied state in QD2, and hence the superconductivity of QD2 is suppressed. It is noticed that $|\langle d_{2\uparrow} d_{2\downarrow}\rangle|$ can be hundreds or even thousands of times of Δ in the original superconductivity, showing that the strength of the secondary proximity effect is significantly high. This behavior may be greatly helpful for achieving topological superconductivity and MZMs.

One can naturally interpret the evolution of the above YSR bound state by considering the energy difference between the ground state and the low excited states of the whole SCDQD system. However, we highlight that since QD1 acts as another new superconducting medium with an energy gap Δ connected directly to QD2 due to the original proximity effect from the S and D electrodes, the above QPT could then be attributed to the competition between superconducting state and side Kondo behavior [65,66] on QD2. The relevant energy scales are the isotropic superconducting gap Δ and the side Kondo temperature of QD2 T_{K2}. Here T_{K2} can be captured by [25,66,67]

$$T_{K2} = U_2\sqrt{\rho J_2}e^{-1/(\rho J_2)}, \tag{3}$$

with $\rho J_2 = 8\Gamma_{c-s}/\pi U_2$ the effective Kondo coupling between QD1 and QD2. The depiction of T_{K2} resembles to the consideration of second-order perturbation theory, as well as the slave-boson mean-field approximation [25]. For parameters given in our present model, the effective hybridization function Γ_{c-s} between two dots can be expressed as [66] $\Gamma_{c-s} = \pi A_1^0(\omega)t^2$. Here, $A_1^0(\omega)$ is the LDOS of QD1 with $t = 0$ and normal conduction leads. With the aid of the Green's function, $A_1^0(\omega)$ could be written as

$$A_1^0(\omega) = \frac{\Gamma}{\pi[(\omega-\varepsilon_1)^2 + \Gamma^2]}. \tag{4}$$

When U_2 is small, such that $T_{K2} > \Delta$, we have a singlet ground state of QD2 ($S_2 = 0$). Whereas if U_2 is large enough with $T_{K2} < \Delta$, the ground state is a spin doublet ($S_2 = 1/2$).

Summarizing the behavior for different superconducting gaps Δ, we then obtain a phase diagram for the singlet and doublet states in Fig. 2(e). It is found that the ground state of QD2 is always a singlet state when U_2 is small. As U_2 increases, it becomes a doublet state. The critical value U_{2c} increases gradually with decreasing Δ. Quite interestingly, in the strong interaction region, the phase boundary relationship between the singlet and doublet ground states could be given by

$$\Delta = 0.7T_{K2}. \tag{5}$$

That is, for $T_{K2}/\Delta > 0.7$, we have a singlet ground state, while for $T_{K2}/\Delta < 0.7$, the ground state is a doublet. However, for smaller U_2, the estimated line deviates from the numerical results, similar to those for the single-impurity case [64,68].

In the aforementioned case, we mainly analyze the secondary proximity effect in QD2 affected by U_2. Now we turn to the case by varying t, with fixed $U_1 = 0$, $U_2 = 0.01$ and $\Delta = 0.0001$ in most instances. From the LDOS of QD2 $A_2(\omega)$ in Fig. 3(a), it can be seen that the YSR peak first moves away from the gap edge to the Fermi surface as t sweeps upwards, and reapproaches the gap edge afterwards. This behavior is well illustrated by Fig. 3(b). For small t, the YSR peaks are located at the edge of the gap. Then they move gradually towards the center if t turns up. Close to the critical value t_c, the ground state switches from a doublet state ($S_2 = 1/2$) to a singlet state ($S_2 = 0$); E_b^+ and E_b^- cross at $t = t_c$. When t is further increased, the YSR peaks move towards the gap edge again and gradually hold there. In Fig. 3(c), we can observe that the weight of the YSR peak shows a tendency

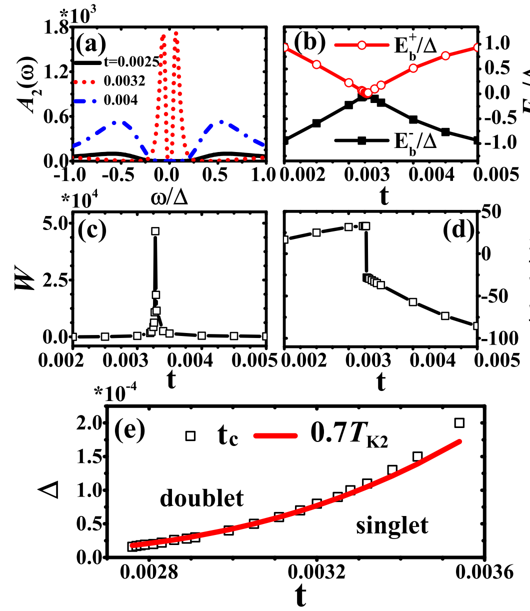

FIG. 3. (a) $A_2(\omega)$ in the gap region $[-\Delta, \Delta]$ for various t with $U_2 = 0.01$ and $\Delta = 0.0001$. (b) $E_b^{\pm}/\Delta$, (c) W, and (d) $\langle d_{2\uparrow}d_{2\downarrow}\rangle/\Delta$ as functions of t. (e) Phase diagram of the singlet and doublet states in the $\Delta - t$ plane. The empty squares describe the critical points t_c for fixed Δ. The red line indicates the fitting function given by Eq. (5). The other parameters are given the same as in Fig. 2 unless specifically stated.

to increase and then decrease with the increasing t, which reaches a maximum at $t_c \approx 0.00328$.

Figure 3(d) depicts $\langle d_{2\uparrow}d_{2\downarrow}\rangle/\Delta$ as a function of t. It is seen that $|\langle d_{2\uparrow}d_{2\downarrow}\rangle|$ gradually strengthens as t increases. Because if t is applied, the particle-hole (p-h) symmetry of both dots is broken, and the probability of the empty or fully occupied states on QD2 increases. When t exceeds t_c, $\langle d_{2\uparrow}d_{2\downarrow}\rangle$ changes abruptly to a negative value, with $|\langle d_{2\uparrow}d_{2\downarrow}\rangle|/\Delta$ enhanced. In this process, J_2 grows progressively with increasing t, resulting in an enlargement of the side Kondo temperature T_{K2} as per Eq. (3). If T_{K2} overwhelms Δ, the binding energy of the Kondo singlet between QD2 and QD1 is favored. So the side Kondo behavior is dominant with the ground state turns to be the singlet $S_2 = 0$ from the doublet $S_2 = 1/2$.

The related phase diagram is plotted in Fig. 3(e). For small t, the ground state of QD2 is always a doublet, whereas if t is large enough, the ground state turns to be a singlet through a QPT. The critical point t_c increases if Δ is lifted up. One observes that t_c could also be well illustrated by Eq. (5); viz., when $\Delta/T_{K2} > 0.7$, the singlet bound state known as the Cooper pair in the QD1 is favored, and the QD2 is in a localized doublet state. Whereas if $\Delta/T_{K2} < 0.7$, the Kondo singlet between two dots is dominant, the side Kondo behavior overwhelms, and the ground state of QD2 changes to a spin singlet.

In Fig. 4(a), we depict the energy dependence of YSR bound states on ε_2 with $U_2 = 0.01$, $t = 0.002$, and $\Delta = 0.001$. It is observed that a pair of YSR resonances appears within the superconducting gap. Due to the p-h symmetry, we only focus on the case $\varepsilon_2 \geqslant -U_2/2$ in the following discussion. As ε_2 increases, the energy of the bound states $|E_b^{\pm}|$ first

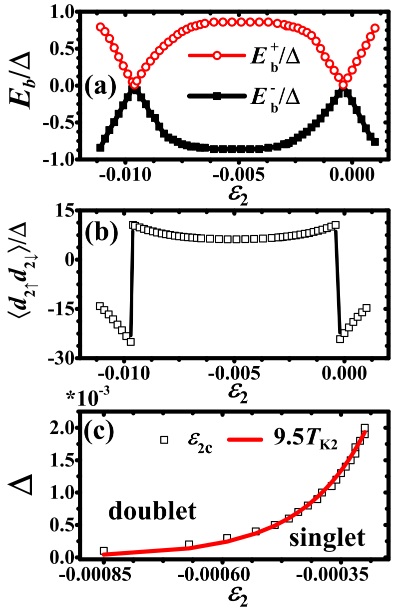

FIG. 4. (a) $E_b^{\pm}/\Delta$ and (b) $\langle d_{2\uparrow}d_{2\downarrow}\rangle/\Delta$ as functions of ε_2 with $U_2 = 0.01$, $t = 0.002$, and $\Delta = 0.001$. (c) Phase diagram of the singlet and doublet states in the $\Delta - \varepsilon_2$ plane. The empty squares describe the critical points in the right side ε_{c2} for fixed Δ. The red line indicates the fitting function given by Eq. (6). The other parameters are given the same as in Fig. 2 unless specifically stated.

decreases toward zero, then gradually increases, indicating a QPT at about $\varepsilon_2 = 0$. Such a QPT could also be found in $|\langle d_{2\uparrow}d_{2\downarrow}\rangle|$; cf. Fig. 4(b). The underlying physical picture for the above phenomenon lies in the following. For parameters given in such a case, and ε_2 is in the singly occupied regime ($\varepsilon_2 \sim -U_2/2$), the ground state of QD2 is a doublet state with $S_2 = 1/2$. When ε_2 is increased, the ground state turns to be a singlet due to QD2 is almost empty.

The phase diagram affected by ε_2 is shown in Fig. 4(c), with a symmetric one occurring around $\varepsilon_2 = -U_2$, but it is not given here. When ε_2 is small, satisfying $-U_2/2 \leqslant \varepsilon_2 < \varepsilon_{2c}$, the ground state is always a doublet state. However, as ε_2 becomes sufficiently large, the ground state undergoes a QPT and transfers into a singlet state, where the critical point ε_{2C} increases for larger Δ. The boundary between the singlet and doublet ground states can be described in terms of Δ and T_{K2}, which can be fitted by

$$\Delta = 9.5T_{K2}. \tag{6}$$

Here, T_{K2} is described by [67,69]

$$T_{K2} = \sqrt{U_2\Gamma_{c-s}} \exp\left[\frac{\pi\varepsilon_2(\varepsilon_2 + U_2)}{U_2\Gamma_{c-s}}\right]. \tag{7}$$

One finds Eq. (7) is consistent with our numerical results.

IV. CONCLUSION

In summary, we have provided an in-depth investigation of the YSR states and the QPTs in a SCDQD device. We have shown that the SCDQD system can be tailored to explore the secondary proximity effect. If QD1 can be treated as a noninteracting resonant level, it triggers an energy gap whose width is nearly the same as the superconducting leads. The YSR peaks could be found in QD2 due to the secondary proximity effect. In such a case, QD1 could be considered as another superconducting lead, and the bound state in QD2 behaves similarly to the case of a single impurity connected to two superconducting leads. The ground state of QD2 undergoes a transformation between a singlet state and a doublet state as the Coulomb repulsion U_2, the interdot coupling strength t, or the energy level ε_2 sweeps. Phase diagrams in the $\Delta - U_2$, $\Delta - t$, and $\Delta - \varepsilon_2$ planes have also been demonstrated, showing that the phase boundaries could be well fitted by $\Delta \approx cT_{K2}$ in all of the above cases, where c is a fitting parameter of order 1.0, similar to the single-impurity case with $c = 0.3$ [64,68]. These findings may show great importance for the design and application of superconducting devices and provide new ideas for further related works. Finally, we stress that in our work, U_1 is fixed at zero because the secondary proximity effect is related to the side Kondo behavior, which is suppressed gradually with increasing U_1 [65,66]. The side Kondo behavior refers to the case where the quantum impurity is connected to a structured nonconstant density of states, differing from the case of the ordinary Kondo effect. For strong U_1, the behaviors may become quite different, which is worthwhile to be studied in any further works.

ACKNOWLEDGMENT

We thank Professor A. A. Aligia for fruitful discussions. This work is supported by the NSFC under Grant No. 12122408, the Natural Science Foundation of Hubei Province under Grants No. 2023AFB456 and No. 2023AFB891, and the open fund of Hubei Key Laboratory of Energy Storage and Power Battery (HUAT) under Grant No. ZDK22023A04.

[1] B. Sacépé, T. Dubouchet, C. Chapelier, M. Sanquer, M. Ovadia, D. Shahar, M. Feigel'man, and L. Ioffe, Localization of preformed Cooper pairs in disordered superconductors, Nat. Phys. **7**, 239 (2011).

[2] G. Z. Wang, T. Dvir, G. P. Mazur, C. X. Liu, N. Loo, S. L. D. ten Haaf, A. Bordin, S. S. Gazibegovic, G. Badawy, E. P. A. M. Bakkers, M. Wimmer, and L. P. Kouwenhoven, Singlet and triplet Cooper pair splitting in hybrid superconducting nanowires, Nature (London) **612**, 448 (2022).

[3] L. Yu, Bound state in superconductors with paramagnetic impurities, Acta Phys. Sin. **21**, 75 (1965).

[4] H. Shiba, Classical spins in superconductors, Prog. Theor. Phys. **40**, 435 (1968).

[5] A. I. Rusinov, On the theory of gapless superconductivity in alloys containing paramagnetic impurities, Sov. J. Exp. Theor. Phys. **29**, 1101 (1969).

[6] V. Mourik, K. Zuo, S. M. Frolov, S. R. Plissard, E. P. A. M. Bakkers, and L. P. Kouwenhoven, Signatures of Majorana

fermions in hybrid superconductor-semiconductor nanowire devices, Science **336**, 1003 (2012).

[7] E. Prada, P. San-Jose, M. W. A. de Moor, A. Geresdi, E. J. H. Lee, J. Klinovaja, D. Loss, J. Nygård, R. Aguado, and L. P. Kouwenhoven, From Andreev to Majorana bound states in hybrid superconductor-semiconductor nanowires, Nat. Rev. Phys. **2**, 575 (2020).

[8] M. Valentini, M. Borovkov, E. Prada, S. Martí-Sánchez, M. Botifoll, A. Hofmann, J. Arbiol, R. Aguado, P. San-Jose, and G. Katsaros, Majorana-like Coulomb spectroscopy in the absence of zero-bias peaks, Nature (London) **612**, 442 (2022).

[9] M. Kheirkhah, D. Zhu, J. Maciejko, and Z. Yan, Corner- and sublattice-sensitive Majorana zero modes on the kagome lattice, Phys. Rev. B **106**, 085420 (2022).

[10] D. Crawford, E. Mascot, M. Shimizu, P. Beck, J. Wiebe, R. Wiesendanger, H. O. Jeschke, D. K. Morr, and S. Rachel, Majorana modes with side features in magnet-superconductor hybrid systems, npj Quantum Mater. **7**, 117 (2022).

[11] Z. Cao, S. Chen, G. Zhang, and D. E. Liu, Recent progress on Majorana in semiconductor-superconductor heterostructures-engineering and detection, Sci. China: Phys. Mech. Astron. **66**, 267003 (2023).

[12] A. Mishra, P. Simon, T. Hyart, and M. Trif, Yu-Shiba-Rusinov qubit, PRX Quantum **2**, 040347 (2021).

[13] L. Pavešić and R. Žitko, Qubit based on spin-singlet Yu-Shiba-Rusinov states, Phys. Rev. B **105**, 075129 (2022).

[14] J. Klinovaja, P. Stano, A. Yazdani, and D. Loss, Topological superconductivity and Majorana fermions in RKKY Systems, Phys. Rev. Lett. **111**, 186805 (2013).

[15] S. Nadj-Perge, I. K. Drozdov, J. Li, H. Chen, S. Jeon, J. Seo, A. H. Macdonald, B. A. Bernevig, and A. Yazdani, Observation of Majorana fermions in ferromagnetic atomic chains on a superconductor, Science **346**, 602 (2014).

[16] B. E. Feldman, M. T. Randeria, J. Li, S. Jeon, Y. Xie, Z. Wang, I. K. Drozdov, B. A. Bernevig, and A. Yazdani, High-resolution studies of the Majorana atomic chain platform, Nat. Phys. **13**, 286 (2017).

[17] G. F. R. Ruiz, M. A. Rampp, A. A. Aligia, J. Schmalian, and L. Arrachea, Josephson junctions of two-dimensional time-reversal invariant superconductors: Signatures of the topological phase, Phys. Rev. B **106**, 195415 (2022).

[18] A. Camjayi, L. Arrachea, A. A. Aligia, and F. von Oppen, Fractional Spin and Josephson effect in time-reversal-invariant topological superconductors, Phys. Rev. Lett. **119**, 046801 (2017).

[19] G. Germanese, F. Paolucci, G. Marchegiani, A. Braggio, and F. Giazotto, Bipolar thermoelectric Josephson engine, Nat. Nanotechnol. **17**, 1084 (2022).

[20] N. Ligato, F. Paolucci, E. Strambini, and F. Giazotto, Thermal superconducting quantum interference proximity transistor, Nat. Phys. **18**, 627 (2022).

[21] Y. Xing, H. Chen, B. Hu, Y. Ye, W. A. Hofer, and H. J. Gao, Reversible switching of Kondo resonance in a single-molecule junction, Nano Res. **15**, 1466 (2022).

[22] S. Kezilebieke, R. Žitko, M. Dvorak, T. Ojanen, and P. Liljeroth, Observation of coexistence of Yu-Shiba-Rusinov states and spin-flip excitations, Nano Lett. **19**, 4614 (2019).

[23] M. T. Deng, C. L. Yu, G. Y. Huang, M. Larsson, P. Caroff, and H. Q. Xu, Anomalous zero-bias conductance peak in a Nb-InSb Nanowire-Nb hybrid device, Nano Lett. **12**, 6414 (2012).

[24] A. Das, Y. Ronen, Y. Most, Y. Oreg, M. Heiblum, and H. Shtrikman, Zero-bias peaks and splitting in an Al-InAs nanowire topological superconductor as a signature of Majorana fermions, Nat. Phys. **8**, 887 (2012).

[25] L. Vaugier, A. A. Aligia, and A. M. Lobos, Spectral density of an interacting dot coupled indirectly to conducting leads, Phys. Rev. B **76**, 165112 (2007).

[26] T. H. Kokkeler, A. A. Golubov, and F. S. Bergeret, Field-free anomalous junction and superconducting diode effect in spin-split superconductor/topological insulator junctions, Phys. Rev. B **106**, 214504 (2022).

[27] J. Chen, W. Xu, Z. Tan, Z. Pan, P. Zhu, Z. M. Liao, and D. Yu, Superconducting proximity in intrinsic magnetic topological insulator $MnBi_2Te_4$ hybrid device modulated by Coulomb blockade effect, Nano Lett. **22**, 6484 (2022).

[28] T. Karabassov, I. V. Bobkova, A. A. Golubov, and A. S. Vasenko, Hybrid helical state and superconducting diode effect in superconductor/ferromagnet/topological insulator heterostructures, Phys. Rev. B **106**, 224509 (2022).

[29] T. Zhou, M. C. Dartiailh, K. Sardashti, J. E. Han, A. Matos-Abiague, J. Shabani, and I. Žutić, Fusion of Majorana bound states with mini-gate control in two-dimensional systems, Nat. Commun. **13**, 1738 (2022).

[30] B. Jäck, Y. Xie, J. Li, S. Jeon, B. A. Bernevig, and A. Yazdani, Observation of a Majorana zero mode in a topologically protected edge channel, Science **364**, 1255 (2019).

[31] L. Du, X. Li, W. Lou, G. Sullivan, K. Chang, J. Kono, and R. R. Du, Evidence for a topological excitonic insulator in InAs/GaSb bilayers, Nat. Commun. **8**, 1971 (2017).

[32] A. I. Buzdin, Proximity effects in superconductorferromagnet heterostructures, Rev. Mod. Phys. **77**, 935 (2005).

[33] J. D. Pillet, P. Joyez, R. Zitko, and M. F. Goffman, Tunneling spectroscopy of a single quantum dot coupled to a superconductor: From Kondo ridge to Andreev bound states, Phys. Rev. B **88**, 045101 (2013).

[34] C. X. Trang, N. Shimamura, K. Nakayama, S. Souma, K. Sugawara, I. Watanabe, K. Yamauchi, T. Oguchi, K. Segawa, T. Takahashi, Y. Ando, and T. Sato, Conversion of a conventional superconductor into a topological superconductor by topological proximity effect, Nat. Commun. **11**, 159 (2020).

[35] S. Kezilebieke, O. J. Silveira, M. N. Huda, V. Vaño, M. Aapro, S. C. Ganguli, J. Lahtinen, R. Mansell, S. van Dijken, A. S. Foster, and P. Liljeroth, Electronic and magnetic characterization of epitaxial $CrBr_3$ monolayers on a superconducting substrate, Adv. Mater. **33**, 2006850 (2021).

[36] L. Schneider, K. T. Ton, I. Ioannidis, J. Neuhaus-Steinmetz, T. Posske, R. Wiesendanger, and J. Wiebe, Proximity superconductivity in atom-by-atom crafted quantum dots, Nature (London) **621**, 60 (2023).

[37] W. S. Cole, J. D. Sau, and S. Das Sarma, Proximity effect and Majorana bound states in clean semiconductor nanowires coupled to disordered superconductors, Phys. Rev. B **94**, 140505(R) (2016).

[38] K. P. Wójcik and I. Weymann, Interplay of the Kondo effect with the induced pairing in electronic and caloric properties of T-shaped double quantum dots, Phys. Rev. B **97**, 235449 (2018).

[39] I. Weymann, K. P. Wójcik, and P. Majek, Majorana-Kondo interplay in T-shaped double quantum dots, Phys. Rev. B **101**, 235404 (2020).

[40] P. Majek, K. P. Wójcik, and I. Weymann, Spin-resolved thermal signatures of Majorana-Kondo interplay in double quantum dots, Phys. Rev. B **105**, 075418 (2022).
[41] J. Barański and T. Domański, Fano-type interference in quantum dots coupled between metallic and superconducting leads, Phys. Rev. B **84**, 195424 (2011).
[42] N. Y. Yao, C. P. Moca, I. Weymann, J. D. Sau, M. D. Lukin, E. A. Demler, and G. Zaránd, Phase diagram and excitations of a Shiba molecule, Phys. Rev. B **90**, 241108(R) (2014).
[43] A. M. Calle, M. Pacheco, G. B. Martins, V. M. Apel, G. A. Lara, and P. A. Orellana, Fano-Andreev effect in a T-shape double quantum dot in the Kondo regime, J. Phys.: Condens. Matter **29**, 135301 (2017).
[44] K. Grove-Rasmussen, G. Steffensen, A. Jellinggaard, M. H. Madsen, R. Žitko, J. Paaske, and J. Nygård, Yu-Shiba-Rusinov screening of spins in double quantum dots, Nat. Commun. **9**, 2376 (2018).
[45] K. P. Wójcik and I. Weymann, Nonlocal pairing as a source of spin exchange and Kondo screening, Phys. Rev. B **99**, 045120 (2019).
[46] B. Baran, R. Taranko, and T. Domański, Subgap dynamics of double quantum dot coupled between superconducting and normal leads, Sci. Rep. **11**, 11138 (2021).
[47] R. Taranko, K. Wrześniewski, B. Baran, I. Weymann, and T. Domański, Transient effects in a double quantum dot sandwiched laterally between superconducting and metallic leads, Phys. Rev. B **103**, 165430 (2021).
[48] M. Žonda, P. Zalom, T. Novotný, G. Loukeris, J. Bätge, and V. Pokorný, Generalized atomic limit of a double quantum dot coupled to superconducting leads, Phys. Rev. B **107**, 115407 (2023).
[49] C. X. Liu, G. Wang, T. Dvir, and M. Wimmer, Tunable superconducting coupling of quantum dots via Andreev bound states in semiconductor-superconductor nanowires, Phys. Rev. Lett. **129**, 267701 (2022).
[50] J. S. Bell, On the problem of hidden variables in quantum mechanics, Rev. Mod. Phys. **38**, 447 (1966).
[51] P. Samuelsson, E. V. Sukhorukov, and M. Büttiker, Orbital entanglement and violation of bell inequalities in mesoscopic conductors, Phys. Rev. Lett. **91**, 157002 (2003).
[52] N. Gisin, G. Ribordy, W. Tittel, and H. Zbinden, Quantum cryptography, Rev. Mod. Phys. **74**, 145 (2002).
[53] C. H. Bennett, G. Brassard, C. Crépeau, R. Jozsa, A. Peres, and W. K. Wootters, Teleporting an unknown quantum state via dual classical and Einstein-Podolsky-Rosen channels, Phys. Rev. Lett. **70**, 1895 (1993).
[54] L. Hofstetter, S. Csonka, J. Nygård, and C. Schönenberger, Cooper pair splitter realized in a two-quantum-dot Y-junction, Nature (London) **461**, 960 (2009).
[55] M. T. Deng, S. Vaitiekėnas, E. B. Hansen, J. Danon, M. Leijnse, K. Flensberg, J. Nygård, P. Krogstrup, and C. M. Marcus, Majorana bound state in a coupled quantum-dot hybrid-nanowire system, Science **354**, 1557 (2016).
[56] B. Pandey, N. Kausha, G. Alvarez, and E. Dagotto, Majorana zero modes in Y-shape interacting Kitaev wires, npj Quantum Mater. **8**, 51 (2023).
[57] J. Barański, T. Zienkiewicz, M. Barańska, K. J. Kapcia, Anomalous Fano resonance in double quantum dot system coupled to superconductor, Sci. Rep. **10**, 2881 (2020).
[58] R. Žitko and T. Pruschke, Energy resolution and discretization artifacts in the numerical renormalization group, Phys. Rev. B **79**, 085106 (2009).
[59] H. R. Krishna-murthy, J. W. Wilkins, and K. G. Wilson, Renormalization-group approach to the Anderson model of dilute magnetic alloys. I. Static properties for the symmetric case, Phys. Rev. B **21**, 1003 (1980).
[60] J. Li, W. D. Schneider, R. Berndt, and B. Delley, Kondo scattering observed at a single magnetic impurity, Phys. Rev. Lett. **80**, 2893 (1998).
[61] V. Madhavan, W. Chen, T. Jamneala, M. Crommie, and N. Wingreen, Tunneling into a single magnetic atom: Spectroscopic evidence of the Kondo resonance, Science **280**, 567 (1998).
[62] R. Bulla, T. A. Costi, and T. Pruschke, Numerical renormalization group method for quantum impurity systems, Rev. Mod. Phys. **80**, 395 (2008).
[63] J. Röntynen and T. Ojanen, Topological superconductivity and high Chern numbers in 2D ferromagnetic Shiba lattices, Phys. Rev. Lett. **114**, 236803 (2015).
[64] J. Bauer, A. Oguri, and A. C. Hewson, Spectral properties of locally correlated electrons in a Bardeen-Cooper-Schrieffer superconductor, J. Phys.: Condens. Matter **19**, 486211 (2007).
[65] L. G. G. V. Dias da Silva, N. P. Sandler, K. Ingersent, and S. E. Ulloa, Zero-field Kondo splitting and quantum-critical transition in double quantum dots, Phys. Rev. Lett. **97**, 096603 (2006).
[66] J. N. Wang, W. H. Zhou, Y. X. Yan, W. Li, N. Nan, J. Zhang, Y. N. Ma, P. C. Wang, X. R. Ma, S. J. Luo, and Y. C. Xiong, Unified formulations for RKKY interaction, side Kondo behavior, and Fano antiresonance in a hybrid tripartite quantum dot device with filtered density of states, Phys. Rev. B **106**, 035428 (2022).
[67] F. D. M. Haldane, Theory of the atomic limit of the Anderson model. I. Perturbation expansions re-examined, J. Phys. C: Solid State Phys. **11**, 5015 (1978).
[68] T. Yoshioka and Y. Ohashi, Numerical renormalization group studies on single impurity Anderson model in superconductivity: A unified treatment of magnetic, nonmagnetic impurities, and resonance scattering, J. Phys. Soc. Jpn. **69**, 1812 (2000).
[69] G. D. Scott and D. Natelson, Kondo resonances in molecular devices, ACS Nano **4**, 3560 (2010).